Short- and long-term behaviours of cantilever-type large-diameter steel tubular pile wall embedded in soft rock against various loadings

S. M. Shafi
Ph.D., Department of Civil and Environmental Engineering, Tokyo Institute of Technology, Tokyo, Japan
J. Takemura
Associate Professor, Department of Civil and Environmental Engineering, Tokyo Institute of Technology, Tokyo, Japan

ABSTRACT

Stability against extreme loads, such as earthquakes, water rise behind the wall and its combination, is a major concern in the application of the cantilever steel tubular pile (CSTP) wall. In the rational design of the CSTP wall against these extreme loadings, one of the critical parameters is the embedment depth and its condition, which is studied in this paper by physical modelling. Centrifuge model tests were carried out to study the stability of the CSTP wall with a retain height H=12m and a pile diameter Φ=2m and thickness, t=25mm subject to extreme loads in 50 g. The embedment condition of two models were single soft rock (q_u=1.4MPa) with rock socket depths (d_r) of 3m and 2.5m, and another one with a rock socketing depth of 2.5m with a 0.5m overlaying sand layer (d_s). Sequential loadings were applied to the wall with dry & saturated backfill sand. It was observed that the stability of the wall against dynamic and static loading increased by a 0.5m increment in rock socketing depth. However, the stability of the wall decreased due to the weathering of the top 0.5m of the shallow rock layer. The resilience effect developed during dynamic loading plays a critical role in determining the wall's behavior under dynamic and static loading.

Key words: *large diameter steel tubular pile, soft rock, centrifuge model, dynamic and static loadings*

1. Introduction

The application of large-diameter cantilever-type steel tubular pile (CSTP) walls as permanent or temporary retain structures has increased in the past decades due to the technological advancement like the rotary cutting press- technique (Miyanohara et al., 2018; Kitamura & Kamimura, 2018; Suzuki & Kimura, 2021; Takemura, 2021) (Fig. 1a). Although the technology has advanced, the design guidelines have not well revised, especially for high stiffness wall embedded into the stiff ground with

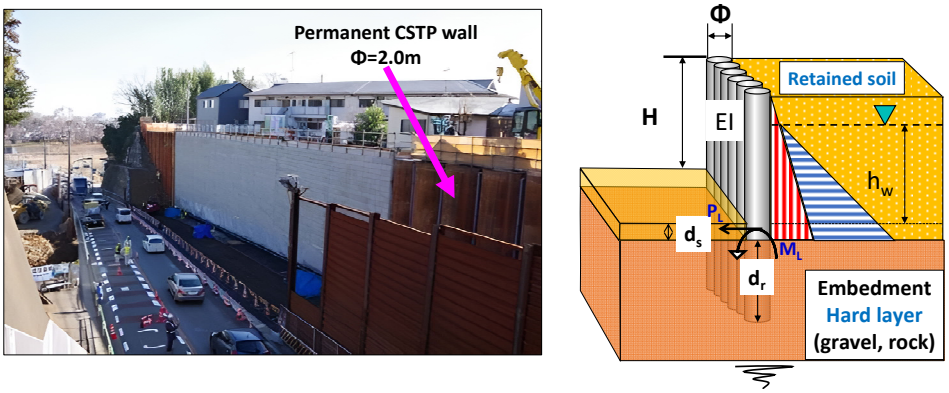

(a) (b)

Fig. 1 Cantilever steel tubular pile (CSTP) wall embedded in hard layer: (a) Application of CSTP wall (Kitamura and Kamimura, 2018); (b) loads expected on CSTP wall during design period

Table 1. Test conditions and the mechanical properties of model CSTP wall, soft rock, and sand

Test code	Embedment soft rock and backfill sand	Rock socket depth: d_r ( )$^{\$}$, [$\beta d_r$]; d_s ( )$^{\$}$ {h_w(m): WR1; h_w:WR2} <FS:h_w(m)=0;WR1;WR2 >	Wall/Pile Properties H, Φ, t, EI, M_y ( )$^{\$}$
Case 1 **C1**	Toyoura sand: (Dr=85%): γ_d=15.8kN/m^3 ϕ'=42° Soft rock: γ_t=20.1kN/m^3 q_u =1.4 Mpa E_{50} = 660 MPa	60 mm (3.0 m) **[1.2]** **{9.6;10.9}** **<2.6;1.1;0.86>**	H= 240mm (12 m) Φ= 40 mm (2.0 m) t= 0.5 mm (25 mm) Spacing: 43 mm (2.15 m) EI= 5.4x10^{-5}GNm^2/m (6.8 GNm^2/m) σ_y= 255 MPa M_y= 3.6x10^{-3} MNm/m (9.0 MNm/m)
Case 3 **C3**		50 mm (2.5 m) **[1.0]** **{8.3;10.3}** **<1.9;0.95;0.69>**	
Case 4 **C4**		50 mm (2.5 m)$^{\$}$; 10 mm ***(0.5 m)*** **{8.9;9.5}** **<1.75;0.78;0.71>**	
$:(prototype scale); βd_r: normalized embedment depth of model CSTP wall (Takemura, 2021)			

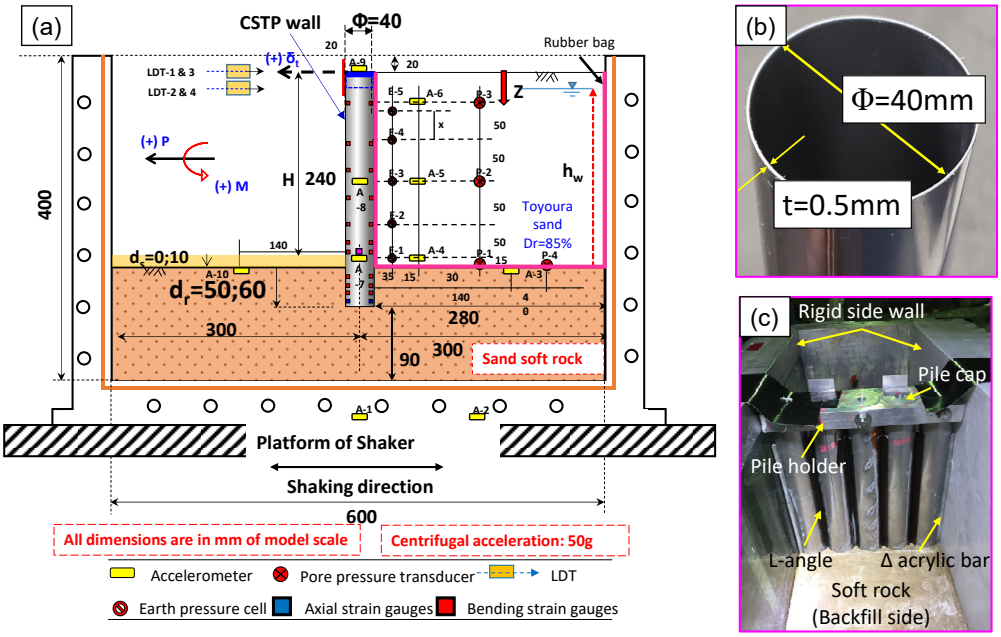

Fig. 2 2D view of the model configuration

large retain height. Also, the behaviour of such walls against extreme loading conditions (large earthquake, buildup of water pressure due to poor drainage conditions or the combination of both, see Fig. 1b) is not well studied (Takemura, 2021). Additionally, for stiff grounds like soft or hard rock, the effect of weathering of the shallow layer needs to be investigated, as small to no lateral resistance could be expected from that weathered layer. To address these concerns, three centrifuge model tests were conducted using Tokyo Tech Mark III centrifuge and the observed results are discussed in this paper.

2. Centrifuge model preparation and test conditions

2.1. Modelling perspective

The test setup of the model is illustrated in Fig. 2a. Considering the specific feature of the CSTP wall and the potential loadings acting on the wall (Fig. 1b), three centrifuge models were made. The effects of the wall embedment were investigated under various loadings. Referring previous centrifuge tests using a 2D plate wall model with similar wall specification (Kunasegaram & Takemura, 2021), which confirmed that the rock socketing depth of d_r=3.0m was able to provide sufficient

stability against the static loading by water rise in the retained soil, d_r=3.0m was employed in the first model. After studying the behaviour, the d_r was further reduced to 2.5m, a 20% reduction in the next model. It should be noted that the normalized embedment depths ($\beta.d_r$) of the two models are 1.2 and 1.0, which are far less than the required d_r in common practice (Takemura, 2021). To discuss the effect of the weathering of the shallow rock layer, a 0.5m overlying sand layer is provided on top of a 2.5m rock socketing depth to have an embedment depth of 3.0m. For the models, a series of dynamic loadings were first applied to the wall with dry retained sand. Then, a static loading was simulated by raising groundwater height in the retained sand. In addition, further dynamic loads were input in the wet sand condition. Interaction between the retained soil and the large diameter CSTP wall was observed during and after loadings to observe the short and long-term behaviours of the wall.

2.2. Model preparation and test conditions

To prepare the model, a rigid frame container (Fig. 2c) with inner dimensions of 600mm x 400mm x 250mm was used. The container width was reduced by attaching a 33mm thick acrylic plate to the backside of the container to tightly accommodate the model wall made of five steel tubular piles. Centrifuge scaling law (Klinkvort et al., 2013; Garnier et al., 2007) was considered for modelling the wall and pile. Each pile has an outer diameter (Φ) of 40mm and thickness (t) of 0.5mm (Φ/t=80), Fig. 2b. The piles were made of stainless steel (SUS304), with Young's modulus (E) of 193 GPa and yield stress of 255 MPa. All the pile and wall properties are reported in Table 1 in model and prototype scale.

The soft rock was prepared with sand-clay cement mixed with the appropriate amount of water, following the mixing ratio used by Kunasegaram & Takemura (2021). The strength and stiffness of the modelled soft rock were determined by conducting the unconfined compressive test on 14th days cured moulded samples. It should be noted that the strength and stiffness of the soft rock depend on various factors like cement quality, temperature, humidity, compaction effort etc. However, to determine the normalized embedment depth (βd_r) and factor of safety, unconfined compressive strength, q_u=1.4 MPa and secant stiffness, E_{50}=660MPa is considered as recommended by Kunasegaram & Takemura (2021). Details about the preparation of the artificial soft rock are reported by Kunasegaram & Takemura (2021).

The soft rock ground was made by compacting the ground layer by layer up to the desired height shown in Fig. 2a. The density of the compacted mixture was carefully controlled by the volume of each compacted layer and the required mass of the mixture for the layer. Before the casting, 0.5 mm thick Teflon sheets were pasted in the front and rear internal container wall faces and lubricated by silicone grease for easy detachment of the wall from the hardened soft rock ground. After making the soft rock layer, the model wall was installed into the unsolidified ground. A guide was used to restrain the horizontal and vertical movement of the wall during the curing period. After that, a wet towel was placed on the ground surface to avoid moisture loss. On the 10th curing day, both the container walls and Teflon sheet were removed, and a new Teflon sheet was attached to the rare wall. The Teflon sheet was not attached to the front wall to secure the view of the model. 5x5 mm mesh was then made on the front of the ground surface to help in the image analysis. L-angle aluminium bars and triangular-shaped acrylic bars were attached to the gaps between the piles and the front/rear walls (Fig. 2c), which were sealed with silicone rubber. Two days before the test, the gap between the wall was closed by silicon paste so that the surface of the wall facing the backfill may become a uniform plane. On the 12th curing day, a rubber bag made of thick latex rubber membrane and a carbon fibre sheet at the base was placed in the retained soil side. By air pluviation technique, Toyoura sand with a relative density (Dr) of 85% was poured into the rubber bag. The side of the rubber bag was smeared with lubricant, and the base was roughened by glueing the sand particle.

Each model was instrumented to measure wall and ground accelerations, wall displacements, lateral earth pressures behind the wall, pore water pressure in the sand, and wall bending strains. The author would like to mention that there is uncertainty in assessing lateral force using the small earth pressure cells for several reasons, such as stress concentration on the cell (Weiler & Kulhawy, 1982), especially near the CSTP wall with a

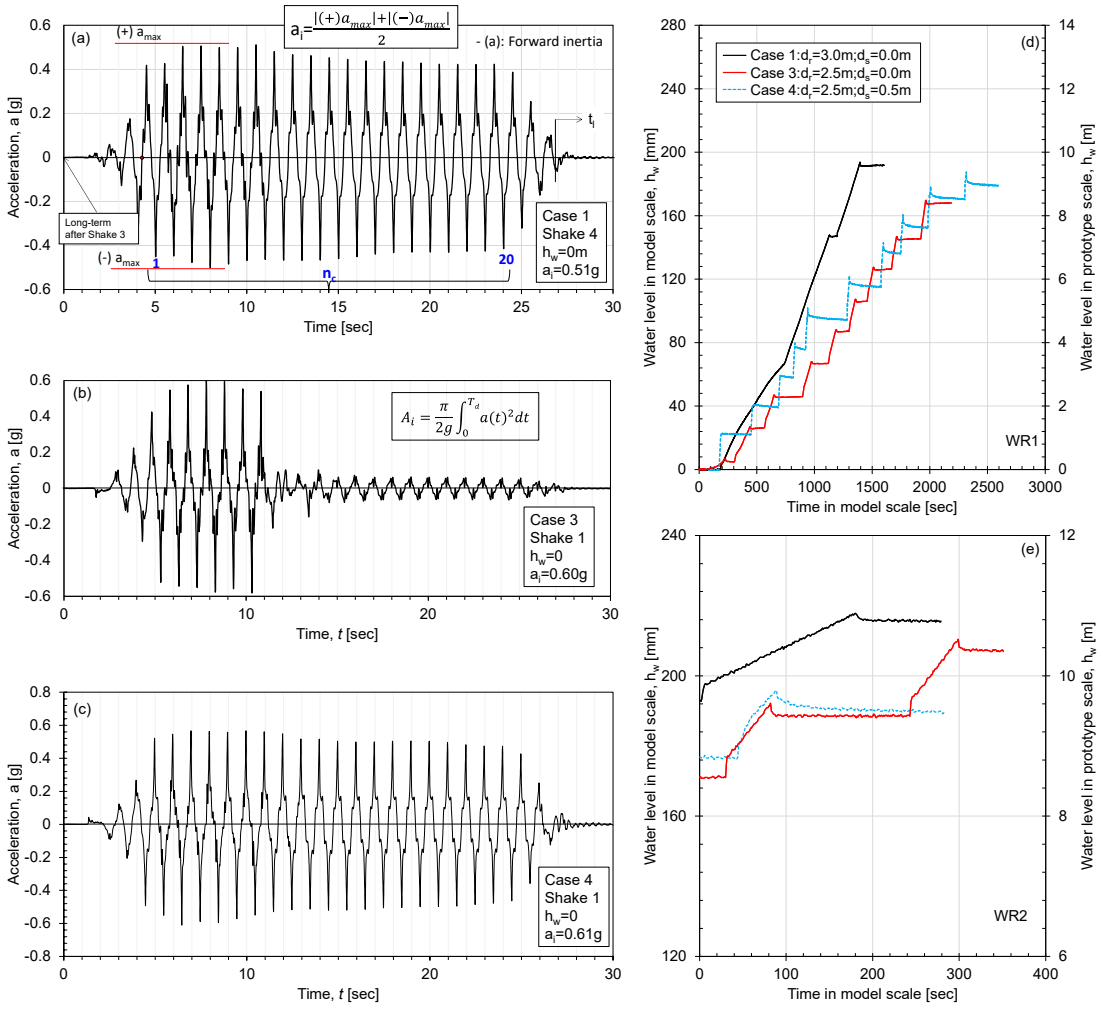

Fig. 3 Typical loadings applied to the CSTP walls (a-c) dynamic loading applied in C1, C3 & C4 (d-e) static loading by water rise

concave/convex surface. Though there are uncertainties in earth pressure measurement, it could provide helpful information about the residual earth pressure acting on the wall after various loadings. The exact location of the EP cell at the top was determined from EP cell and PPT measurement. The distance' x' in Fig. 2a was 35mm, 30mm, and 40mm for Cases 1,3 and 4, respectively.

The details of the test conditions are given in Table 1. Two tests were conducted using single soft rock layer with rock socketing depths (d_r) of 3m (Case 1) and 2.5m (Case 3). Another test was conducted with a rock socketing depth of 2.5m with a 0.5m overlaying sand layer (d_s) (Case 4) in prototype scale. Case 2 with single soft rock layer and rock socket depths (d_r) of 2.5m is excluded form reporting as the experiment failed due to the poor performance of the centrifuge shaker and sensors. In Case 4, on the experiment day, sand at the top fell outside the rubber bag and stuck with the grease smeared on the container wall. Also, a small leak in the rubber bag was confirmed from the measurement.

The factor of safety against rotation at different water levels (h_w) was calculated using the moment minimization technique explained by Madabhushi & Chandrasekaran (2005) and reported in **Table 1**.

A sinusoidal wave of a predominant frequency of 1Hz was used as dynamic loading, as shown in Fig. 3(a-c). Static loading was applied by supplying water in the back, as shown in Fig. 3 (d-e). In total, water level (h_w) over 3H/4 was achieved by two times the water supply. The details about the loading sequence and histories are given in Fig. 4. The amplitude of the input motion (a_i) was calculated as defined in Fig. 3a, and (a_i) of all shakings are given in Fig. 4. The effective number of the cycle (cycles with almost same magnitude) is termed as 'n_c' in this paper and shown in Fig. 4. Due to the number of cycles variation, Arias intensity (A_i)

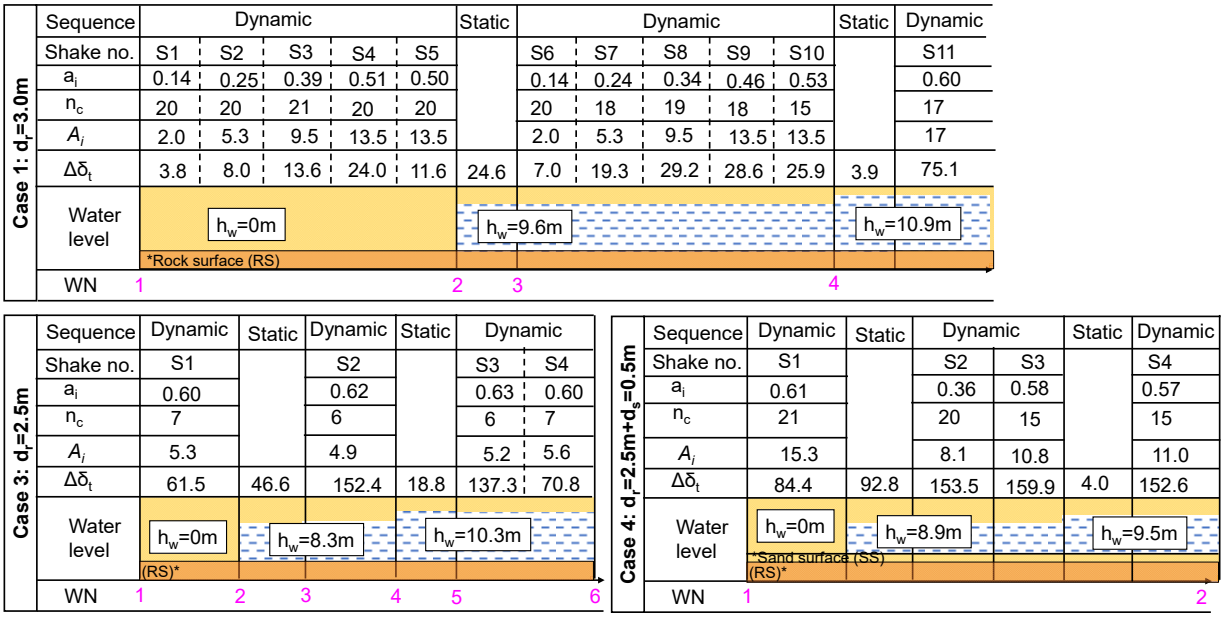

a_i: absolute max. amplitude of input motion [g]; n_c: number of effective cycles; A_i: Arias Intensity [m/sec] $\Delta\delta_t$: wall top displacement increment [mm]; WN: White noise

Fig. 4 Details about the loading sequence and histories followed in Cases 1, 3 and 4

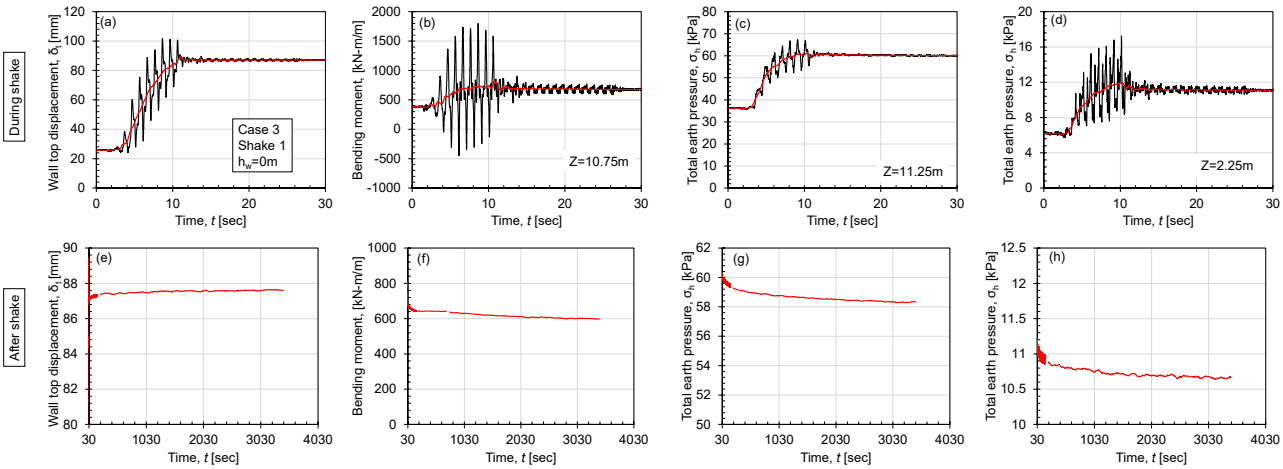

Fig. 5 Examples of typical measurements during and after shaking Case 3 shake 1: (a,e) wall top displacement; (b,f) bending moment at Z=10.75m; (c,g) total earth pressures at Z=11.25m; (d,h) total earth pressure at Z=2.25m

(defined in Fig. 3b) is used as a reference value and given in Fig. 4.

The following sections include the test result and discussion. Unless stated otherwise, all the values are given in the prototype scale.

3. Centrifuge test results & discussions

3.1. Typical time history of centrifuge measurement

A typical time history of measured wall top displacement (δ_t), bending moment (BM) at Z=10.75m and total earth pressure (σ_h) at two different depths (Z=2.25 & 11.25m) from Case 3 shake 1 are shown in Fig. 4. The accumulation of kinematic or the residual component is indicated by the solid red line. The measurement is shown in two parts: during shaking (Fig. 5 (a-d)) and after shaking (Fig. 5 (e-h)). During shaking δ_t, BM, and σ_h increased. However, a small increment in δt caused the reduction of BM and σh after shaking.

For high-stiffness walls securely embedded in the stiff ground, the 'elastic resilience' of the wall influences the 'ratcheting effect' (Hirakawa et al., 2007; Tatsuoka et al., 2003), which could cause the increase in σ_h with δ_t during dynamic loading. However, a small increment in δ_t in the long term could reduce the elastic resilience effect of the wall.

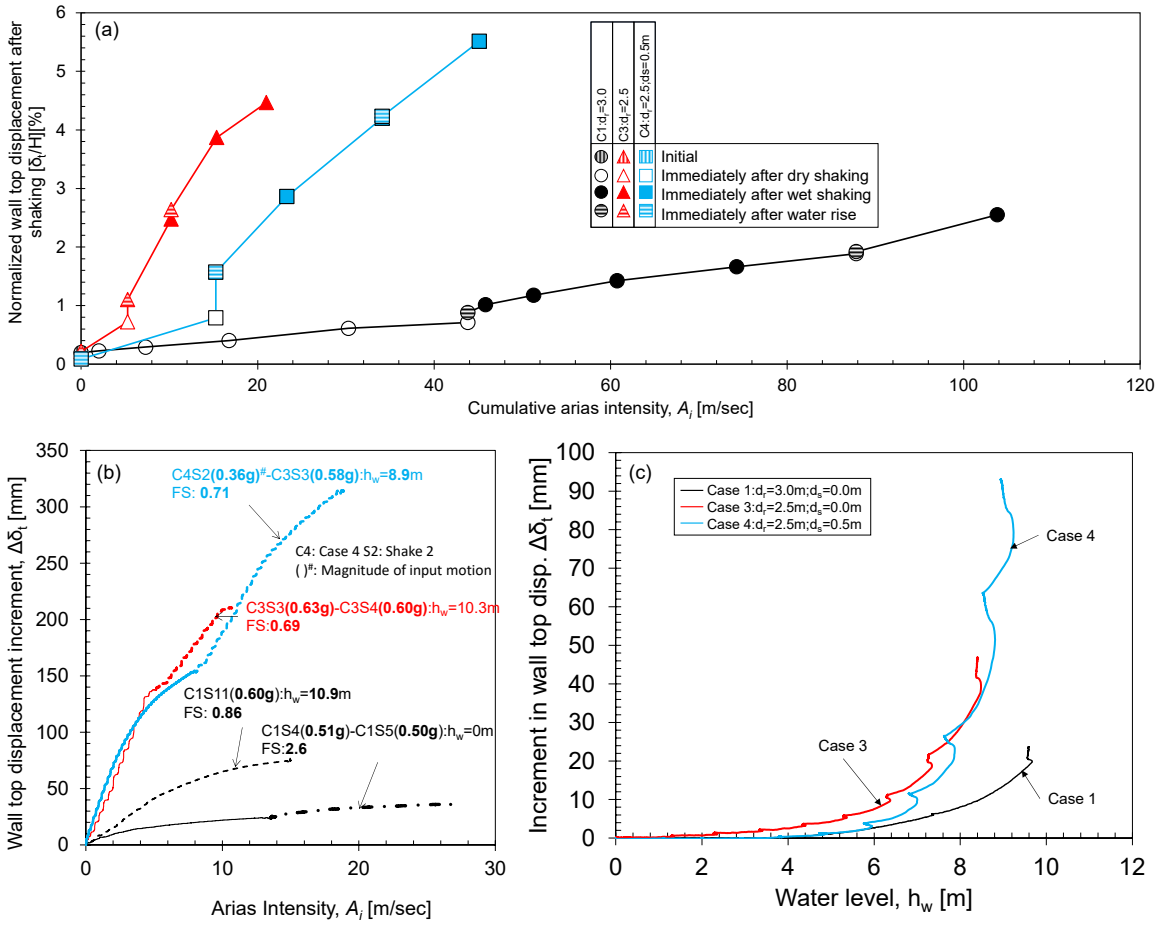

Fig. 6 Wall top displacement variation (a) during dynamic loading (b) during static loading

3.2. Wall displacement variation of CSTP wall under dynamic and static loadings

The entire wall displacement variation of CSTP walls by dynamic and static loadings in Cases 1,3 and 4 is plotted against the cumulative arias intensity in Fig. 6a. The residual wall top displacement accumulates after each loading. In all three cases, the residual wall top displacement was larger than 2%H, the allowable limit given by IPA (2016) for level II earthquake. Overall, the final residual wall top displacement is larger for case 4, followed by case 3 then case 1. To know more about wall displacement behaviour during dynamic loading, the increment of wall displacement during dynamic loadings is plotted against the Arias intensity in Fig. 6b. The wall displacement for consecutive shakings under similar water levels is plotted continuously against the Arias intensity. Similarly, to know the wall displacement during static loading by water rise, the increment in wall displacement is plotted against the water level in Fig. 6c.

A nonlinear variation of wall displacement with Arias intensity was observed during dynamic loadings from all cases (Fig. 6b). Comparing C1S11 and C4S2-C4S3, for identical Arias intensity, the observed wall displacement was larger for Case 4 than Case 1. Although the water level in Case 1 was 1m higher than in Case 4, the factor of safety in Case 1 was 20% larger than in Case 4. The 20% difference in factor of safety caused more than 3.5 times wall top displacement (at Arias intensity 15m/sec) in case 4 than in case 1. Similarly, comparing C4S11 with the C3S3-C3S4, the wall displacement was larger for Case 3 than for Case 1. Although the water level and the safety factor were 5% and 20% larger in Case 1 than in Case 3, the wall displacement was about 2.5 times larger in Case 3 than in Case 1. The increment in displacement during C1S5 was smaller than C1S4. Similarly, C3S4 showed a smaller displacement increment compared to C3S3. This observation can be interpreted as if the subsequent input motion is smaller than the previous input motion; the wall displacement during the latter would be smaller than the previous. No significant difference was observed between case 3 and case 4 up to A_i=10m/sec.

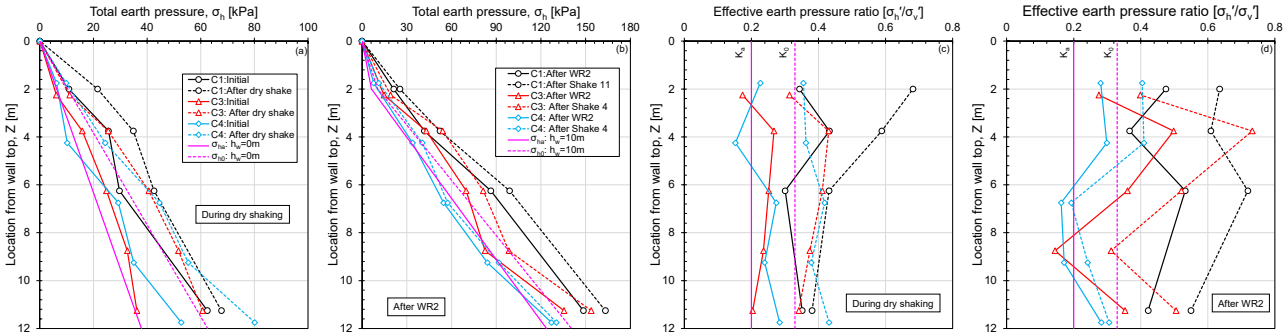

Fig. 7 Horizontal earth pressure distribution with depth (a,b) total earth pressure (c,d) effective earth pressure ratio

A nonlinear variation of wall displacements with water levels was observed during dynamic loadings from all cases (Fig. 6c). At small water levels (h_w<4m), no significant increase in wall displacement was observed. This observation can be interpreted as due to the resilience effect from the previous dynamic loading; the large earth pressure (Fig. 7) prevented the wall from instantaneously initiating the active condition, resulting in a small wall displacement. However, at a larger water level (h_w>8m), a sharp increase in wall displacement was confirmed for Cases 3 and 4. Overall, the observed displacement during case 1 was smaller than in Cases 3 and 4. Furthermore, no significant difference was confirmed between case 3 and case 4 up to h_w=8m.

From Fig. 6, it can be said that increasing the rock socketing depth by 0.5m could significantly reduce the wall displacement. Also, a 0.5m weathering of shallow rock layers could increase the wall displacement.

3.3. Earth pressure behaviour of CSTP walls

Although there are some uncertainties related to the earth pressure measurement by the small earth pressure cell (Weiler & Kulhawy, 1982), the measured earth pressure could provide useful insights into understanding the behaviour of CSTP walls under sequential loadings.

The horizontal earth pressure distributions with depths are shown in Fig. 7. Fig. 7a-b shows the total earth pressure distribution with depth during dry shaking and final shaking of Cases 1,3 and 4. On the other hand, Fig. 7c-d shows the effective earth pressure ratio distribution with depth under similar conditions. Two reference lines are drawn to indicate the total active (σ_{ha}) and at-rest (σ_{h0}) pressure distribution at h_w=0m and 10m, respectively, in Fig. 7a-b. Similarly, two reference lines are drawn to indicate the active (K_a) and at-rest (K_0) earth pressure coefficient in Fig. 7c-d. The initial total earth pressure observed from Cases 1, 3 and 4 was larger than the active earth pressure (Fig. 7a). After the end of dry shaking, the total earth pressure increased more than the at-rest pressure. After the final loading (Fig. 7b), Cases 1 and 3 showed more than at-rest pressure in almost all the locations. However, case 4 showed less than at-rest conditions, especially at Z=6.75m. The effective earth pressure ratio distribution can provide a clearer understanding of the earth pressure behaviour. The horizontal effective earth pressure was calculated by subtracting the static water pressure from the total earth pressure. Then, the ratio (σ_h'/σ_v') was obtained by dividing the horizontal effective earth pressure by the vertical effective earth pressure.

The ratios observed initially and after dry shaking of cases, 3 and 4 were almost similar. After the dry shaking, a ratio of more than K_0 was observed for Cases 3 and 4. On the other hand, the ratio observed in case 1 after dry shaking was much larger than in cases 3 and 4, especially at shallower depths. After the final loading, the earth pressure ratio of more than K_0 can be confirmed for Cases 1 and 3. However, the Case 4 ratio was smaller than K_0, especially at the deeper depth.

3.4. Bending moment behaviour of CSTP walls

The bending moment distributions with depth for Cases 1 and 3 are shown in Fgi.8. Case 4 is excluded for bending moment distribution, as many strain gauges failed during the test. Two reference lines are drawn from the active (M_a) and at-rest (M_0) total earth pressure distribution at h_w=0m, 10.3m and 10.9m.

A much smaller initial bending moment was observed in Case 3 than in Case 1, which was less than the M_a. The maximum bending moment should be expected at the rock surface for a cantilever retaining wall. However, the maximum bending moment in Case 1

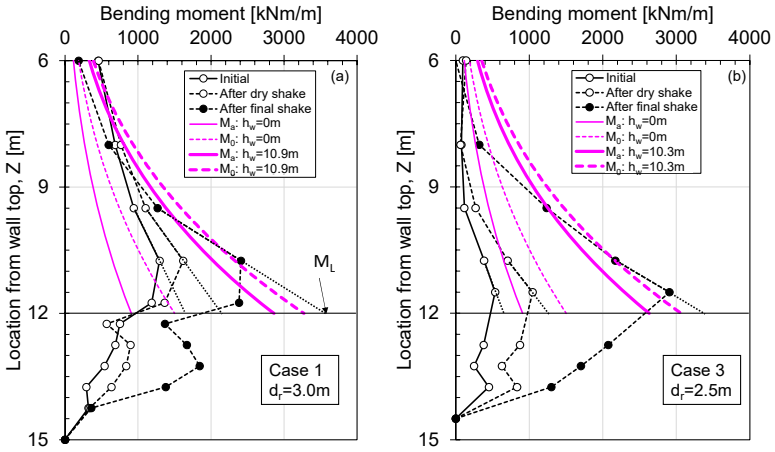

Fig. 8 Bending moment distributions with depth (a) Case l; d_r=3.0m (b) Case 3; d_r=2.5m

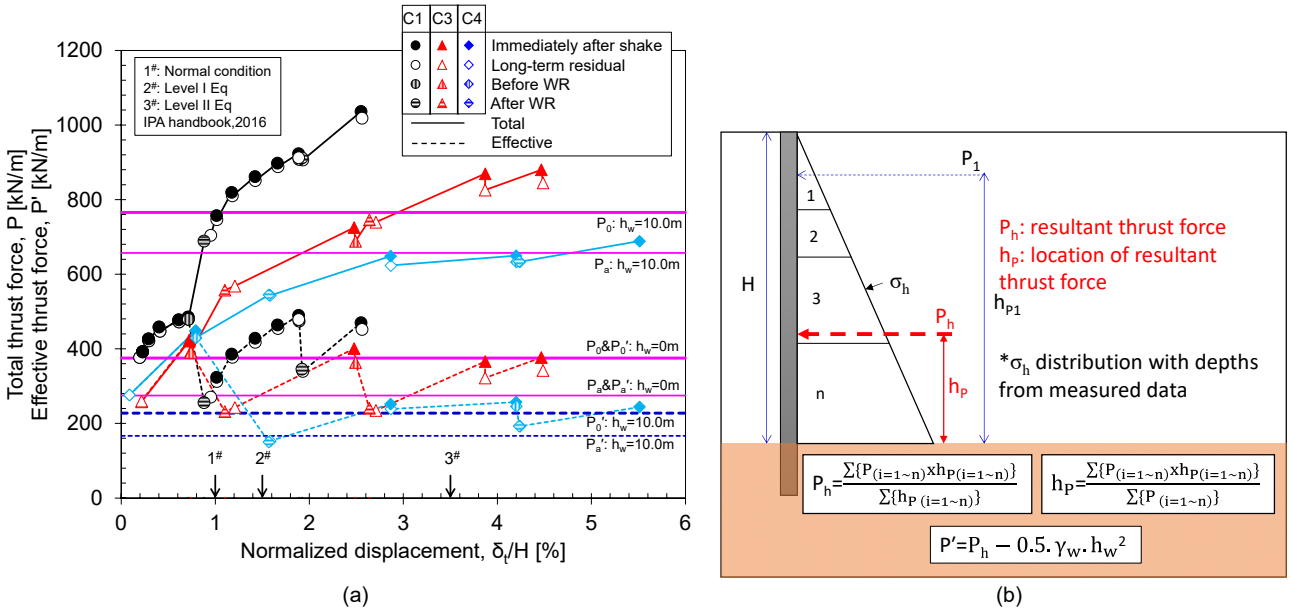

Fig. 9 Effect of embedment conditions on the thrust force

was observed at Z=10.75m instead of 11.75m, which could be due to the stress concentration (Ishihama et al., 2020) near the rock surface. The bending moment at Z=10.75m in Case 1 was more than M_0, but for Case 3, it was close to M_a after dry shaking. After final shaking, both Cases 1 and 3 showed a bending moment about M_0 at Z=10.75m. The equivalent moment load (M_L) was calculated by linearly extrapolating the bending moment at Z=10.75 and 9.5m for Case 1 and Z=10.75 and 11.5m for Case 3, as shown in Fig.8. M_L obtained after the dry and final shake from Case 1 was larger than Case 3. The difference of M_L between Case 1 and 3 after the dry shake was larger than after the final shake, which can be interpreted as a small displacement level; the effect of a 0.5m change in rock socketing depth would be much larger compared to a larger displacement level.

3.5. Effect of embedment conditions on the CSTP wall behaviour

The total and effective thrust force variation with wall displacement for cases 1,3 and 4 are shown in Fig. 9a. Following Fig. 9b, the total thrust force was calculated from the total earth pressure distribution. The effective thrust force was calculated by subtracting the thrust force obtained from hydrostatic pressure. Reference lines are drawn to indicate the active (P_a & P_a') and at-rest (P_0 & P_0') total and effective thrust force at h_w=0 and 10m.

The increase in total and effective thrust force with wall displacement was observed in all shakings. After the water rises, the effective thrust force is reduced to P_a for all cases. In the long term, a small increase in the wall displacement reduced the total and effective thrust force.

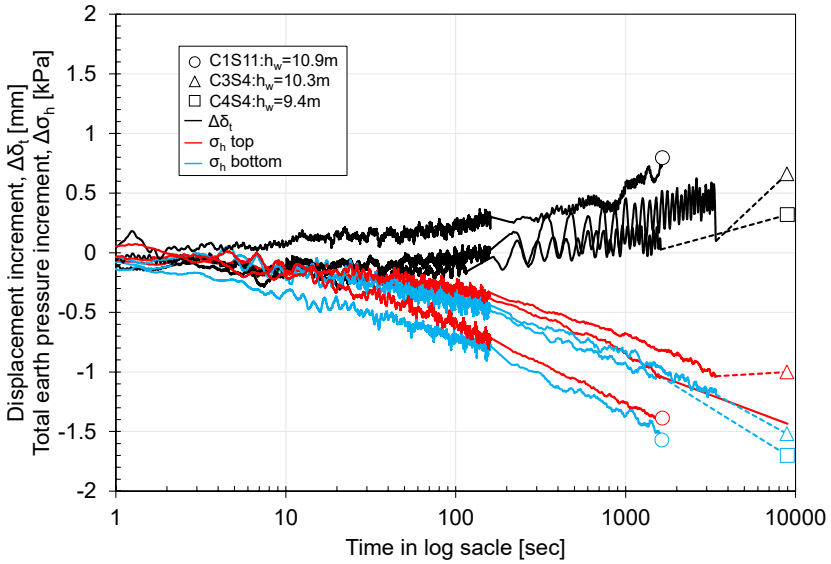

Fig. 10 Long-term behavior (displacement, earth pressure) of the CSTP wall after final loadings

The decrement in the total and effective thrust force was much larger in Case 3, shake 3 and 4 than in other cases. After the dry shaking, an effective thrust force of more than P_0' was observed in all the cases. After the final loading, the total and effective thrust force more than the at-rest force was observed for all cases. Overall, the observed thrust force was much larger for Case 1 than for Case 3 and 4. Therefore, a weathering of 0.5m shallow rock layer could significantly reduce the thrust force acting on the wall. Also, a 0.5m decrease in rock socketing depth could reduce the thrust force significantly. At displacement less than normal condition (1%H), no significant difference was observed between Case 3 and Case 4, although the safety margin was larger for Case 3 than Case 4. However, a clear difference becomes visible between cases 3 and 4 as the imposed displacement increases. After the final loading, the observed displacement was larger for case 4 than for case 3 and case 1. Although the wall displacement of more than the allowable displacement (example: Level 1 earthquake by IPA handbook, (2016)) was observed in all cases, the increase in the thrust force during final shaking indicates the presence of resilience effect. This indicates the presence of a secured rock-wall confinement condition. Furthermore, designing the wall using design active or at-rest conditions could underestimate the force acting on the CSTP wall.

3.6. Long-term behaviour of CSTP wall

For less redundant structures like CSTP walls with large retain height, the long-term behaviour needs to be investigated (Takemura, 2021). The wall displacement and total earth pressure variation with time after loading (t_l, shown in Fig. 3a) are shown in Fig. 10. The variations are shown for final loading. A displacement increment by creep can be seen in all cases. The creep displacement was negligible compared to the displacement during shaking. The forward creep displacement caused the decrease in the total earth pressure, which reduces the larger earth pressure caused by the resilience effect. However, earth pressure more than active pressure was seen after the final loading (Fig. 7d). Larger creep displacement was observed after the water rise, especially after WR1 of cases 1 and 3 (Fig. 9a). No significant effect of the rock socketing depth was seen on the creep displacement after the dynamic loading of Cases 1 and 3. From Fig. 9 and 10, it can be said that the long-term creep displacement is less severe after the dynamic loading than the static loading due to the resilience effect.

4. Conclusions

Three centrifuge model tests were conducted under 50g centrifugal acceleration. The model wall was made of steel tubular pipes (2m diameter (Φ) and 25mm thickness (t) in prototype scale) with a retaining wall height (H) of 12m. Three different wall embedment depths (d_e) were made. Two models were single soft rock (q_u=1.4MPa) with rock socket depths (d_r) of 3m and 2.5m, and one with a rock d_r of 2.5m with a 0.5m overlaying sand layer (d_s). Sequential loadings were

applied to the wall with dry and wet backfill sand. From these tests, the following conclusions are derived:

1. Changes in rock conditions, such as increasing the depth of rock socketing or weathering of the rock layer, can significantly impact wall displacement.
2. For high-stiffness walls embedded into the stiff ground with good confinement conditions, the residual effective earth pressure increases with the wall displacement by dynamic loadings, defined as the "elastic resilience effect" in this study. The resilience effect plays a critical role in CSTP wall behaviour under sequential loadings. Under sequential extreme loading conditions, the effective earth pressure ratio (σ_h'/σ_v') kept increasing (more than commonly used K_a and K_0) even at wall displacement more than the allowable wall displacement given in the IPA handbook (2016), which suggests that the assumed design earth pressure might underestimate the wall bending moment.
3. The long-term creep displacement will be more concern after static loading than dynamic loading due to the reduction of earth pressure developed by the resilience effect. Also, the embedment condition might not significantly affect the long-term creep displacement.

5. Acknowledgements

The authors gratefully acknowledge the individual advice and guidance provided by the members and advisers of the IPA TC1 (Committee on the application of cantilever-type steel tubular pile wall embedded in the stiff ground) in connection with the preparation of this paper.

References

Garnier, J., Gaudin, C., Springman, S.M., Culligan, P.J., Goodings, D., Konig, D., Kutter, B., Phillips, R., Randolph, M.F., Thorel, L., 2007. Catalogue of scaling laws and similitude questions in geotechnical centrifuge modelling. International Journal of Physical Modelling in Geotechnics 7, 01–23. https://doi.org/10.1680/ijpmg.2007.070301

Gopal Madabhushi, S.P., Chandrasekaran, V.S., 2005. Rotation of Cantilever Sheet Pile Walls. J. Geotech. Geoenviron. Eng. 131, 202–212. https://doi.org/10.1061/(ASCE)1090-0241(2005)131:2(202)

Hirakawa, D., Nojiri, M., Aizawa, H., Tatsuoka, F., Sumiyoshi, T., Uchimura, T., 2007. Residual Earth Pressure on a Retaining Wall with Sand Backfill Subjected to Forced Cyclic Lateral Displacements, in: Ling, H.I., Callisto, L., Leshchinsky, D., Koseki, J. (Eds.), Soil Stress-Strain Behavior: Measurement, Modeling and Analysis, Solid Mechanics and Its Applications. Springer Netherlands, Dordrecht, pp. 865–874. https://doi.org/10.1007/978-1-4020-6146-2_65

Klinkvort, R.T., Hededal, O., Springman, S.M., 2013. Scaling issues in centrifuge modelling of monopiles. International Journal of Physical Modelling in Geotechnics 13, 38–49. https://doi.org/10.1680/ijpmg.12.00010

Kunasegaram, V., Takemura, J., 2021. Deflection and failure of high-stiffness cantilever retaining wall embedded in soft rock. International Journal of Physical Modelling in Geotechnics 21, 114–134. https://doi.org/10.1680/jphmg.19.00008

MIYANOHARA, T., KUROSAWA, T., HARATA, N., KITAMURA, K., SUZUKI, N., KAJINO, K., 2018. Overview of the Self-standing and High Stiffness Tubular Pile Walls in Japan. https://doi.org/10.50876/icpe.1.0_167

Suzuki, N., Kimura, Y., 2021. Summary of case histories of retaining wall installed by rotary cutting press-in method, in: Proceedings of the Second International Conference on Press-in Engineering 2021, Kochi, Japan. CRC Press, pp. 581–587.

Takemura, J., 2021. State of the art report on application of cantilever type steel tubular pile wall embedded to stiff grounds, in: Proceedings of the Second International Conference on Press-in Engineering 2021, Kochi, Japan. CRC Press, pp. 27–41.

Tatsuoka, F., Masuda, T., Siddiquee, M.S.A., Koseki, J., 2003. Modeling the Stress-Strain Relations of Sand in Cyclic Plane Strain Loading. J. Geotech. Geoenviron. Eng. 129, 450–467. https://doi.org/10.1061/(ASCE)1090-0241(2003)129:6(450)

Weiler, W.A., Kulhawy, F.H., 1982. Factors Affecting Stress Cell Measurements in Soil. J. Geotech. Engrg. Div. 108, 1529–1548. https://doi.org/10.1061/AJGEB6.0001393